Dating paleochannel iron ore by (U-Th)/He analysis of supergene goethite, Hamersley province, Australia

Jonathan A. Heim
Paulo M. Vasconcelos
Earth Sciences, University of Queensland, Brisbane, Queensland 4072, Australia
David L. Shuster*
Kenneth A. Farley
Geological and Planetary Sciences, California Institute of Technology, Pasadena, California 91125, USA
G. Broadbent Rio Tinto Exploration—Australasia Region, 37 Belmont Avenue, Belmont, WA 6104, Australia

ABSTRACT

(U-Th)/He dating of late-stage authigenic goethite, combined with corrections for diffusive loss of ^{4}He by the ^{4}He/^{3}He methodology, reveals strong correlation between a sample's age and its depth in ferruginized channel sediments from the Yandicoogina deposit, Western Australia. Corrected ages, ranging from ca. 18 Ma near the surface to ca. 5 Ma at the bottom of the profile, indicate that ferruginization of the aggraded channels becomes progressively younger with depth. This trend is consistent with goethite precipitation at the groundwater-atmosphere interface during water table drawdown driven by the aridification of Western Australia during the Neogene. The results demonstrate that the (U-Th)/He system is ideal for dating goethite if diffusive loss corrections are applied. The approach is suitable for dating weathering reactions on Earth and should also be suitable for dating Fe oxyhydroxides in the Martian regolith.

Keywords: (U-Th)/He dating, goethite, weathering geochronology, channel iron deposits, iron ore.

INTRODUCTION

Ancient river channels in the Hamersley province, Western Australia (Fig. 1A), contain such large concentrations of ferruginized sediments that they constitute high-grade goethite-hematite ore. This style of mineralization, channel iron deposits (CID), supplies 40–50% of the iron currently mined in Australia. The widespread occurrence, considerable length (>100 km), gentle gradients (<2 m/km), and meandering courses of these paleochannels suggest they were mature river systems draining an extensive area of Hamersley. Following their incision, sometime in the past, the channels were aggraded with fragments of iron-rich detrital material, wood, and banded iron-formation. After aggradation, the sediments were Fe-metasomatized. The controlling mechanisms and timing of channel aggradation and ferruginization remain controversial (see references in Morris et al., 1993, and Ramanaidou et al., 2003). Determining the age of aggradation is difficult because the sediments are extremely oxidized and afossiliferous. Pollens extracted from clay horizons at the base of the channel reveal that aggradation may have started at the Eocene-Oligocene transition ca. 34–36 Ma, in response to major disruption of global climates and ocean circulation patterns (MacPhail and Stone, 2004). Climate instability was triggered by the onset of rapid seafloor spreading in the Southern Ocean, which also accelerated the northward drift of Australia (Veevers et al., 1991). However, the end of aggradation and the main phase of goethite cementation of channel sediments are not known.

Recently, Shuster et al. (2005) demonstrated that supergene goethite is suitable for (U-Th)/He dating if partial ^{4}He losses are quantified by the ^{4}He/^{3}He method. We employed this approach to determine the timing and duration of goethite precipitation and to evaluate possible mechanisms controlling ferruginization of the aggraded channel sediments at the Yandicoogina (Yandi) deposit, a prominent CID at Hamersley (Figs. 1A–1D). Goethite precipitation ages constrain the timing of ferruginization and concurrent removal of Si, Al, and other elements. Dating ferruginization of channel sediments provides a minimum age for the end of channel aggradation. In addition, the geochronological results may contribute in determining the climatic conditions promoting aggradation and ferruginization of paleochannels in Western Australia.

GEOLOGY OF THE YANDI CHANNEL IRON DEPOSIT

The Yandi paleochannel is an ~90-km-long, almost continuous concentration of high-grade pisolitic iron ore with low P and Al_2O_3 contents (58–60% Fe, ~0.05% P, 1–2% Al_2O_3, 3–5% SiO_2, ~10% loss on ignition [LOI]). Mining exposures show the ferruginized channel to be ~500–600 m wide and 50–70 m deep (Fig. 1C). The main ore horizon (Barimunya member) overlies basal clay and conglomerates (Munjina member) and is di-

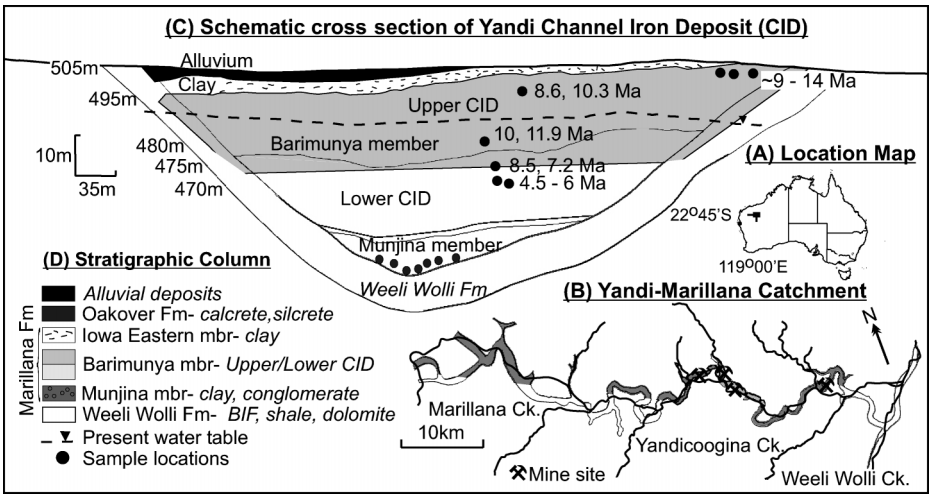

Figure 1. Location (A) and plan view (B) of Yandi catchment, illustrating the mature nature of CID paleochannels in Hamersley, Western Australia. Schematic cross section (C) and stratigraphic column (D) through Yandi channel show positions of goethite samples (black dots) and their uncorrected (U-Th)/He ages. (Modified from Ramanaidou et al., 2003.) CID—channel iron deposit; Fm—Formation; mbr—member; BIF—banded-iron formation; Ck—Creek.

*Present address: Berkeley Geochronology Center, 2455 Ridge Road, Berkeley, California 94709, USA

TABLE 1. (U-Th)/He RESULTS

Sample	Age* (MA)	±	Th/U	LRD† % He loss	High-Retentivity Domain						RL (m)
					5% He loss		10% He loss		20% He loss		
					§Age_{corr} (Ma)	±	Age_{corr} (Ma)	±	Age_{corr} (Ma)	±	
Yan02-01-A(a)	10.0	0.3	1.08	*3*#	10.8	0.9	*11.4*	*1.4*	13.1	3.2	500
Yan02-01-A(b)**	nd	nd	0.64	*3*	nd	nd	nd	nd	nd	nd	500
Yan02-01-B(b)**	9.4	0.3	1.24	5	10.4	1.0	11.0	1.6	12.3	3.0	500
Yan02-01-D1(c)	13.6	0.4	0.29	*5*#	15.0	1.5	*15.9*	*2.3*	17.8	4.3	500
Yan02-01-D1(d)	13.3	0.4	0.29	*5*#	14.7	1.4	*15.5*	*2.2*	17.5	4.2	500
Yan02-01-D2(c)	10.7	0.3	0.47	*5*#	11.8	1.2	12.5	1.8	*14.0*	*3.4*	500
Yan02-01-D2(d)	11.0	0.3	0.47	*5*#	12.2	1.2	12.8	1.9	*14.5*	*3.5*	500
Yan02-02-1(b)	10.3	0.3	2.23	5	11.5	1.1	12.1	1.8	13.6	3.3	495
Yan02-02-1(a)	8.6	0.3	1.54	5	9.5	0.9	10.0	1.5	11.3	2.7	495
Yan02-03(a)	11.9	0.4	2.10	5	13.2	1.3	14.0	2.0	15.7	3.8	480
Yan02-03(b)	10.0	0.3	1.52	5	11.1	1.1	11.7	1.7	13.2	3.2	480
Yan02-08-4(a)	8.5	0.3	0.20	5	9.5	0.9	10.0	1.5	11.2	2.7	475
Yan02-08-4(b)	7.2	0.2	0.14	5	7.9	0.8	8.4	1.2	9.4	2.3	475
Yan02-04-A(a)	4.6	0.1	0.22	5	5.1	0.5	5.3	0.8	6.0	1.4	470
Yan02-04-A(b)	5.8	0.2	0.36	5	6.5	0.6	6.8	1.0	7.7	1.8	470
Yan02-05(a)	4.4	0.1	0.29	5	4.9	0.5	5.2	0.8	5.8	1.4	470
Yan02-05(b)	5.0	0.1	0.38	5	5.5	0.5	5.8	0.8	6.5	1.6	470
Yan02-06(a)	11.7	0.4	0.77	5	13.0	1.3	13.7	2.0	15.4	3.7	nd
Yan02-06(b)	12.9	0.4	1.06	5	14.3	1.4	15.1	2.2	17.0	4.1	nd
Yan02-09-A(a)	6.3	0.2	0.20	5	7.0	0.7	7.4	1.1	8.3	2.0	nd
Yan02-09-A(b)	7.9	0.2	0.25	5	8.7	0.9	9.2	1.3	10.3	2.5	nd

*(U-Th)/He ages not corrected for partial diffusive helium loss.
†Low-retention helium domain (LRD).
§Age_{corr}: ages corrected for partial diffusive ^{4}He loss using a 2 domain spherical diffusion model.
#He loss quantified by modelling of results obtained from ^{4}He/^{3}He diffusion experiments[2].
**Duplicate aliquot lost during automated sample processing, resulting in only one (U-Th)/He age.
RL = Reference Elevation; nd = no data.

vided into upper and lower CID (Ramanaidou et al., 2003) (Figs. 1C and 1D). CID ore comprises predominantly ooids (<2 mm) and pisoids (>2 mm) with hematite or goethite nuclei concentrically rimmed (cortex) by layers of vitreous goethite (Ramanaidou et al., 2003). Rounded to angular fragments (1–10 mm) of hematite, goethite, and maghemite, often rimmed by a thin goethite cortex, also constitute the channel fill (Ramanaidou et al., 2003). Wood fragments (1 mm to ~5 cm) replaced by goethite, or rarely by hematite, are abundant, but larger branches or trunks are rare. Late-stage massive and botryoidal vitreous goethite cements channel sediments, forming the ore matrix (Ramanaidou et al., 2003). Post ferruginization weathering has partially destroyed the characteristic CID texture in near-surface horizons. The upper CID is also more jointed and cavernous, hosting vertical solution pipes locally lined or infilled by clay, botryoidal goethite, and opaline silica.

METHODS

Ten samples of iron ore fragments, eight of which represent a vertical section through the Yandi channel (Fig. 1C), were cut into 15 × 10 × 2 cm blocks and polished to expose different generations of iron oxides (see GSA Data Repository[1]. Drill cores (4 mm diameter) recovered vitreous goethite cement from each sample. Drill cores were crushed to 0.1–3 mm fragments, sieved, and ultrasonically cleaned in ethanol. From each sample, five to ten fragments, devoid of detrital phases, were selected for geochronology, and a similar number were polished for scanning electron microscope (SEM) and electron microprobe (EMP) analyses; 50–100 fragments of goethite were powdered for X-ray diffraction (XRD) analyses.

A single goethite fragment from each sample was split into two aliquots (5–50 μg), then inserted in a small Pt tube and heated with a Nd-YAG laser at the California Institute of Technology (Caltech) following the procedures of Farley (2002) and Shuster et al. (2005). Other goethite grains were bombarded with 220 MeV protons at the Northeast Proton Therapy Center, and the irradiated grains were incrementally heated using a low-temperature extraction cell described by Farley et al. (1999). The released gas fractions were analyzed for ^{3}He and ^{4}He following the procedures of Shuster et al. (2004). After complete degassing, goethite grains were transferred to a Teflon beaker containing ^{230}Th and ^{235}U spikes and dissolved by concentrated HCl and heating for 12 h to 90 °C. The spiked solutions were analyzed for ^{238}U and ^{232}Th by double-focusing inductively coupled plasma–mass spectrometry (ICP-MS).

RESULTS AND DISCUSSION

Microscopy

Petrographic analyses indicate that vitreous goethite is a late-stage phase cementing channel sediments; it is also the predominant mineral replacing primary rock fragments or forming cortices surrounding pisoids and ooids. SEM analyses show that all grains from the recovered drill cores are polycrystalline, where 1–10 μm prismatic goethite crystals are oriented perpendicularly to the growth plane, forming 1–10 μm-thick layers. Accretionary growth of these layers creates the banded or botryoidal textures characteristic of goethite cements in CID ores. Each growth band represents one event of goethite precipitation, and 0.1–3 mm grains may host ten to 3000 such bands, depending on the size of the crystals. This indicates that grains dated by the (U-Th)/He method may contain several generations of goethite. EMP analyses show that Al substitution, which may lower the crystallinity of goethite (Schulze and Schwertmann, 1984) and decrease ^{4}He retentivity, is limited (1–5 wt% Al). XRD results yield narrow, sharp, and symmetrical peaks, suggesting a high degree of crystallinity; Rietveld analysis yields a narrow range of unit cell parameters (a = 4.59–4.61 Å, b = 9.91–9.95 Å, c = 3.01–3.02 Å).

(U-Th)/He Results

(U-Th)/He results are listed in Table 1. Based on the reproducibility of in-house standards, the precision of the He determinations is ~3% (2σ). Since errors introduced by the U and Th ICP-MS analyses are insignificant, a 3% uncertainty is a reasonable estimate for the analytical error in age determinations. To assess external reproducibility, we analyzed two aliquots of goethite from each sample. None of the samples analyzed in duplicate yields statistically reproducible results, which we attribute to three possible explanations: (1) Goethite does not quantitatively retain ^{4}He; (2) goethite either loses or gains U and Th after precipitation; (3) the subsamples analyzed for each fragment represent distinct growth bands and were precipitated at different times in the past.

We tested hypothesis (1), the most likely source of error in the goethite (U-Th)/He age (Shuster et al., 2005), by analyzing proton-irradiated grains using the ^{4}He/^{3}He method, following the procedures of Shuster et al. (2004). The results yield well-defined arrays in ^{3}He Arrhenius plots, suggesting that two characteristic diffusion domains exist within each sample: low-retentivity domains (LRD) with high He diffusivity containing no ^{4}He, and high-retentivity domains (HRD), which presently contain all of the radiogenic ^{4}He in the samples (Appendix 2 [see footnote 1]). Discrepancy between the ^{4}He and ^{3}He release fractions reveals a nonuniform distribution of radiogenic ^{4}He within the HRD of each sample. Modeling of the spatial distribution of ^{4}He within the HRD, and assuming (1) a uni-

[1]GSA Data Repository item 2006032, Appendices 1 and 2, is available online at www.geosociety.org/pubs/ft2006.htm, or on request from editing@geosociety.org or Documents Secretary, GSA, P.O. Box 9140, Boulder, CO 80301, USA.

form distribution of proton-induced ^{3}He, and (2) that only two isolated diffusion domains are present in each sample (Shuster et al., 2005), indicates that two of the goethite samples (Yan02–01-D1, Yan02–01-A) diffusively lost ~10% of the ^{4}He during radiogenic ingrowth. Another sample (Yan02–01-D2) lost ~20% ^{4}He.

We use our ^{4}He/^{3}He diffusion experiments to estimate the maximum possible diffusive loss of He for each sample and to estimate age uncertainties arising from these losses. Corrections are applied to the He abundances by accounting for the deficit gas fraction in the LRD and HRD; these corrected He abundances are used to calculate corrected (U-Th)/He ages. Error bars are estimated to be the total age correction. When we apply similar age corrections to all samples, the results become statistically reproducible between aliquots (Table 1), suggesting that ^{4}He loss may indeed account for the apparent age discrepancies. Age reproducibility suggests that (U-Th)/He dating of supergene goethite yields reliable precipitation ages when corrected for diffusive loss of ^{4}He.

Comparing ages obtained from multiple samples collected at close proximity in the profile provides an additional test of whether the (U-Th)/He dates represent true mineral precipitation ages. Assuming the worst-case scenario of 20% He loss in error calculation, two samples from the 470 m mining bench yield four dates (6.0 ± 1.4, 7.7 ± 1.8, 5.8 ± 1.4, and 6.5 ± 1.6 Ma), indistinguishable at the 2σ confidence level. Four samples from the 500 m bench level also yield reproducible ages (13.1 ± 3.2, 12.3 ± 3.0, 17.8 ± 4.3, 17.5 ± 4.2, 14.0 ± 3.4, and 14.5 ± 3.5 Ma) at the 2σ confidence interval. Random samples (Yan02-06 and Yan02-09-A) collected elsewhere in the deposit yield ages (15.4 ± 3.7 and 17.0 ± 4.1 Ma; 8.3 ± 2.0 and 10.3 ± 2.5 Ma) that are compatible with ages obtained for the vertical traverse and suggest that the (U-Th)/He results are internally consistent and reveal mineral precipitation ages.

Figure 2 illustrates another significant trend in the uncorrected and corrected ages. Age versus depth diagrams show a progressive decrease in a sample's age with increasing profile depth. Best-fit lines for uncorrected ages, and ages corrected for 5, 10, and 20% ^{4}He losses, yield moderate correlation lines ($R^2 \approx 0.6$) with slopes ranging from 3.6 m/m.y. for no ^{4}He loss correction to 3.2, 3.1, and 2.7 m/m.y. for 5%, 10%, and 20% ^{4}He loss corrections, respectively. Such decrease in a sample's age with increasing depth in the profile has been observed in other studies (Vasconcelos and Conroy, 2003; Carmo and Vasconcelos, 2005). The age distribution in Figure 2 could indicate fast downward propagation of a goethite precipitation front at ca. 18 Ma and a decrease in the front propagation rate from 15 to 5 Ma. Alternatively, the age distribution in the diagrams may suggest the presence of two distinct age populations, which correspond to the texturally and mineralogically distinct upper and lower CID deposits. Textural differences, where recrystallization features are common in the upper CID but less pronounced in the lower CID, suggest that the lower CID may define a homogenous goethite population, while the upper CID deposit may represent the dissolution and reprecipitation of earlier goethite cement. Best-fit curves through the lower CID results (Fig. 2) reveal excellent correlations ($R^2 = 0.93$ for 5%, 10%, and 20% ^{4}He loss corrections, respectively), yielding slopes of 1.54, 1.39, 1.32, and 1.17 m/m.y. These diagrams reveal two possible age populations: a CID goethite cement population that follows an age-versus-elevation curve with slope of ~1.2–1.5 m/m.y., and an upper CID goethite cement population offset toward younger ages from this curve (Fig. 2). Extrapolating the low CID ages to the original surface (~505 m) yields an age intercept of ca. 28–36 Ma, consistent with the palynological ages (MacPhail and Stone, 2004) obtained from clay sediments at the bottom of the channel.

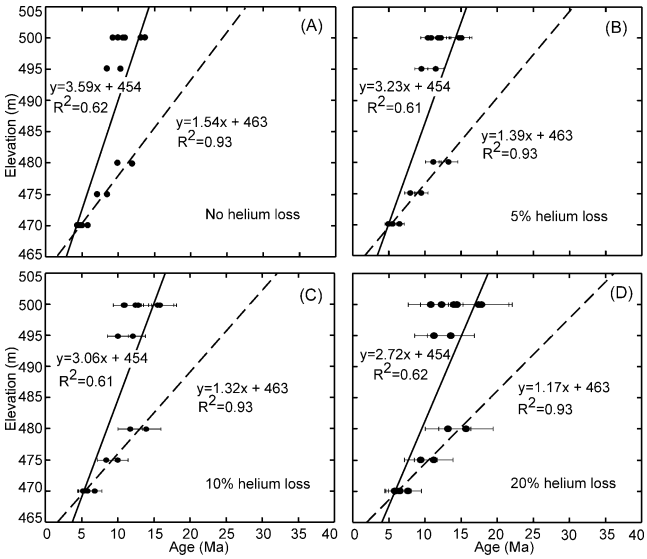

Figure 2. Goethite elevation versus (U-Th)/He ages for (A) uncorrected ages, and ages corrected for (B) 5%, (C) 10%, and (D) 20% ^{4}He losses, showing that the results are statistically reproducible (2σ) when corrected for 10 and 20% ^{4}He losses. Linear regression curves (solid lines) of all samples for each plot show progressively younger results with increasing profile depth ($R^2 \approx 0.61$). Correlation coefficients are much greater ($R^2 = 0.93$) if only lower CID samples are plotted (dashed lines), suggesting the presence of two age populations (see text). Extrapolating the younger results, corrected for 20% ^{4}He losses, to the original channel surface (~505 m) shows an intercept at 36 Ma, consistent with palynological ages for the initiation of channel aggradation (MacPhail and Stone, 2004). Upper CID samples are offset from this trend, suggesting partial dissolution and reprecipitation of goethite cement near the surface, possibly associated with excursion to more humid climates in the Miocene (McGowran et al., 1997).

Generation of CID Deposits

The mature nature of the paleochannels and their width and moderate slopes suggest that the CID drainage evolved under more humid conditions than those present in Western Australia today. Early Oligocene pollen assemblages at the bottom of the channel suggest a cooler and wetter climate during sedimentation (MacPhail and Stone, 2004). Channel aggradation indicates that, after the Early Oligocene, a transition toward arid conditions, combined with rapid erosion of previously formed weathering profiles and weathered bedrock, filled the channels with detrital components. A large percentage of this detritus is composed of Fe-rich clasts (fragments of previously formed ferruginous duricrusts or partially weathered, banded iron-formation) and wood fragments. Therefore, channel aggradation must have been fast, leading to quick burial of rock and wood fragments before plant detritus had time to decay. Aggradation must have occurred during onset of aridity, which also prevented erosion of the aggraded channels. Due to their morphology and the porosity/permeability contrast with the surrounding country rock, the aggraded channels were likely the locus of groundwater accumulation and subsurface flow. Interaction with abundant buried organic matter would have caused groundwater to become acidic and reducing, promoting the partial dissolution of Fe-rich fragments. Soluble Fe^{2+} would then quickly oxidize to Fe^{3+} and reprecipitate as goethite cement at the groundwater-atmosphere interface:

1. Reductive dissolution of hematite

$$Fe_2O_{3(\text{hematite})} + HCOOH_{(\text{carboxylic acid})} + 4H^+_{(aq)} \Leftrightarrow 2Fe^{2+}_{(aq)} + CO_{2(aq)} + 3H_2O_{(l)}$$

2. Direct precipitation of goethite (ferruginization)

$$2Fe^{2+}_{(aq)} + 0.5O_{2(aq)} + 3H_2O_{(l)} \Leftrightarrow 2FeOOH_{(\text{goethite})} + 4H^+_{(aq)}$$

Geochemical conditions conducive to channel ferruginization also apparently promoted wood fossilization. Pseudomorphic replacement of organic matter by goethite requires groundwater-saturated conditions to prevent organic matter decomposition and to provide a continuous supply of ions for replacement (Wopfner, 1983). Below, we suggest a mechanism by which this may have occurred.

During chemical weathering, elements not sensitive to redox reactions remained in solution and were leached from the system. Collapse due to volume reduction would destroy original textures of large clasts or ferruginized wood. With increased aridity throughout the Neogene, the process of iron cementation at the groundwater-atmosphere interface apparently moved downward, following the progressive deepening of the water table through time. Tectonic uplift could also cause deepening of the water table, but evidence for uplift at this time is missing. Extrapolation of the age versus elevation trend from the bottom of the profile to the present surface (505 m) suggests that ferruginization may have started at ca. 36 Ma, immediately after the aggradation of the channel. These results indicate that the water table deepened at a rate of ~1.2–1.5 m/m.y. from ca. 36 Ma onwards. Eventually, the entire channel fill would have become ferruginized. This process appears to have continued throughout the Neogene, with goethite precipitation occurring at the bottom of the profile in the Pliocene and possibly more recently.

The deviation from the age versus elevation trend observed for the upper CID samples suggests that subsequent to goethite cementation, the upper CID underwent partial dissolution and secondary precipitation of younger generations of goethite cements. This event, possibly associated with more humid conditions during the Miocene (McGowran et al., 1997), is also suggested by the vertical solution pipes, clay infills, and late-stage silica in the upper CID. Our proposed scenario for ferruginization during water table descent also implies that the water table dropped to depths ~60 m below the present surface (reference elevation = 445 m) by the time channel ferruginization ceased, sometime after the Pliocene. Since the present water table lies at ~485 m elevation, the water table appears to have raised ~40 m since the channel was completely ferruginized. This rise in water table implies that Western Australia experienced wetter conditions in the recent past than in the Pliocene, an interpretation consistent with the northward movement of Australia into the Indian Ocean monsoon belt.

CONCLUSION

When corrected for partial diffusive loss of ^{4}He, (U-Th)/He ages of goethite cements from the Yandi CID in Western Australia are progressively younger with depth. This trend strongly suggests that the iron cementation process was driven by drawdown of the water table through the Neogene, with goethite cementation occurring at the paleo-groundwater–atmosphere interface. The trend also suggests that the CID formed by the in situ dissolution and reprecipitation of iron within an aggraded channel by saturated groundwater enriched in organic acids. Rapid aggradation, combined with anaerobic conditions, created acidic-reducing groundwaters in the channel due to the large proportion of detrital wood and plant matter. The water table deepened as Western Australia evolved toward greater aridity throughout the Neogene. Partial destruction of the CID textures in the upper CID and deviation of upper CID ages from the age versus depth trend at the bottom of the profile suggest that a brief excursion to more humid conditions in the Miocene (McGowran et al., 1997) promoted the partial recrystallization of early goethite cements in the near-surface environment. Another transition toward more humid conditions in the recent past is also implied by the rise of the water table from the deepest ferruginized sediments to its present level. The results presented here further substantiate previous conclusions that goethite is suitable for (U-Th)/He dating (Lippolt et al., 1998; Shuster et al., 2005), and illustrate the need to correct goethite He ages for incomplete ^{4}He retentivity using the ^{4}He/^{3}He methodology. Goethite dating by the ^{4}He/^{3}He variant of the (U-Th)/He method is an ideal approach for studying weathering processes on Earth and, given new evidence for the presence of goethite on the Martian regolith, possibly on Mars.

ACKNOWLEDGMENTS

We thank Rio Tinto Exploration Pty. Limited, and Hamersley Iron Pty. Limited, for logistic support, University of Queensland (UQ) Centre for Microcopy and Microanalysis staff for help during microanalysis, Peter Colls for sample preparation, and Janet Sisterson for help with the proton irradiation. This project was partially funded by the UQ-Argon Geochronology in Earth Sciences (UQ-AGES) laboratory, a UQ Graduate School Scholarship to Heim, and the National Science Foundation. B. Kohn, D. Phillips, and an anonymous reviewer provided constructive comments.

REFERENCES CITED

Carmo, I.O., and Vasconcelos, P.M., 2006, ^{40}Ar/^{39}Ar geochronology constraints on late Miocene weathering rates in Minas Gerais, Brazil: Earth and Planetary Science Letters, v. 241, p. 80–94.

Farley, K.A., 2002, (U-Th)/He dating: Techniques, Calibrations, and Applications, *in* Porcelli, D., et al., eds., Reviews in mineralogy and geochemistry: Noble gases in geochemistry and cosmochemistry, Volume 47: Washington, Mineralogical Society of America, p. 819–844.

Farley, K.A., Reiners, P.W., and Nenow, V., 1999, An apparatus for high precision helium diffusion measurements from minerals: Analytical Chemistry, v. 71, p. 2059–2061, doi: 10.1021/ac9813078.

Lippolt, H.J., Brander, T., and Mankopf, N.R., 1998, An attempt to determine formation ages of goethites and limonites by (U-Th)/^{4}He dating: Neues Jahrbuch für Mineralogie-Monatshefte, v. 11, p. 505–528.

MacPhail, M.K., and Stone, M.S., 2004, Age and palaeoenvironmental constraints on the genesis of the Yandi channel iron deposits, Marillana Formation, Pilbara, northwestern Australia: Australian Journal of Earth Sciences, v. 51, p. 497–520, doi: 10.1111/j.1400-0952.2004.01071.x.

McGowran, B., Li, Q., Cann, J., Padley, D., McKirdy, D.M., and Shafik, S., 1997, Biogeographic impact of the Leeuwin Current in southern Australia since the late middle Eocene: Palaeogeography, Palaeoclimatology, Palaeoecology, v. 136, p. 19–40, doi: 10.1016/S0031-0182(97)00073-4.

Morris, R.C., Ramanaidou, E.R., and Horwitz, R.C., 1993, Channel iron deposits of the Hamersley province: Commonwealth Scientific and Industrial Research Organisation Exploration and Mining Restricted Report 399R.

Ramanaidou, E.R., Morris, R.C., and Horwitz, R.C., 2003, Channel iron deposits of the Hamersley province, Western Australia: Australian Journal of Earth Sciences, v. 50, p. 669–690, doi: 10.1111/j.1440-0952.2003.01019.x.

Schulze, D.G., and Schwertmann, U., 1984, The influence of aluminum on iron-oxides, X: Properties of Al-substituted goethites: Clay Minerals, v. 19, p. 521–539.

Shuster, D.L., Farley, K.A., Sisterson, J., and Burnett, D.S., 2004, Quantifying the diffusion kinetics and spatial distributions of radiogenic ^{4}He in minerals containing proton-induced ^{3}He: Earth and Planetary Science Letters, v. 217, p. 19–32, doi: 10.1016/S0012-821X(03)00594-6.

Shuster, D.L., Vasconcelos, P.M., Heim, J.A., and Farley, K.A., 2005, Weathering geochronology by (U-Th)/He dating of goethite: Geochimica et Cosmochimica Acta, v. 69, p. 659–673, doi: 10.1016/j.gca.2004.07.028.

Vasconcelos, P.M., and Conroy, M., 2003, Geochronology of weathering and landscape evolution, Dugald River valley, NW Queensland, Australia: Geochimica et Cosmochimica Acta, v. 67, p. 2913–2930, doi: 10.1016/S0016-7037(02)01372-8.

Veevers, J.J., Powell, C.M., and Roots, S.R., 1991, Review of sea-floor spreading around Australia, I: Synthesis of the patterns of spreading: Australian Journal of Earth Sciences, v. 38, p. 373–389.

Wopfner, H., 1983, Kaolinisation and the formation of silicified wood on Late Jurassic Gondwana surfaces, *in* Wilson, R.C.L., ed., Residual deposits: Surface related weathering processes and materials, Volume 11: London, Geological Society of London, p. 27–31.

Manuscript received 13 July 2005
Revised manuscript received 9 November 2005
Manuscript accepted 14 November 2005

Printed in USA